The Astrophysical Journal Letters, 942:L25 (7pp), 2023 January 10 https://doi.org/10.3847/2041-8213/acaaac

Early Results from GLASS-JWST. IX. First Spectroscopic Confirmation of Low-mass Quiescent Galaxies at $z > 2$ with NIRISS

Danilo Marchesini[1], Gabriel Brammer[2,3], Takahiro Morishita[4], Pietro Bergamini[5,6], Xin Wang[7], Marusa Bradac[8,9], Guido Roberts-Borsani[10], Victoria Strait[2,3], Tommaso Treu[10], Adriano Fontana[11], Tucker Jones[9], Paola Santini[11], Benedetta Vulcani[12], Ana Acebron[5,13], Antonello Calabrò[11], Marco Castellano[11], Karl Glazebrook[14], Claudio Grillo[5,13], Amata Mercurio[15,17], Themiya Nanayakkara[14], Piero Rosati[6,16], Chanita Tubthong[1], and Eros Vanzella[6]

[1] Physics and Astronomy Department, Tufts University, 574 Boston Avenue, Medford, MA 02155, USA; danilo.marchesini@tufts.edu
[2] Cosmic Dawn Center (DAWN), Denmark
[3] Niels Bohr Institute, University of Copenhagen, Jagtvej 128, DK-2200 Copenhagen N, Denmark
[4] IPAC, California Institute of Technology, MC 314-6, 1200 E. California Boulevard, Pasadena, CA 91125, USA
[5] Dipartimento di Fisica, Università degli Studi di Milano, Via Celoria 16, I-20133 Milano, Italy
[6] INAF—OAS, Osservatorio di Astrofisica e Scienza dello Spazio di Bologna, via Gobetti 93/3, I-40129 Bologna, Italy
[7] Infrared Processing and Analysis Center, Caltech, 1200 E. California Blvd., Pasadena, CA 91125, USA
[8] Department of Mathematics and Physics, University of Ljubljana, Jadranska ulica 19, SI-1000 Ljubljana, Slovenia
[9] Department of Physics and Astronomy, University of California, Davis, 1 Shields Avenue, Davis, CA 95616, USA
[10] Department of Physics and Astronomy, University of California, Los Angeles, 430 Portola Plaza, Los Angeles, CA 90095, USA
[11] INAF Osservatorio Astronomico di Roma, Via Frascati 33, I-00078 Monteporzio Catone, Rome, Italy
[12] INAF Osservatorio Astronomico di Padova, vicolo dell'Osservatorio 5, I-35122 Padova, Italy
[13] INAF—IASF Milano, via A. Corti 12, I-20133 Milano, Italy
[14] Centre for Astrophysics and Supercomputing, Swinburne University of Technology, P.O. Box 218, Hawthorn, VIC 3122, Australia
[15] INAF—Osservatorio Astronomico di Capodimonte, Via Moiariello 16, I-80131 Napoli, Italy
[16] Dipartimento di Fisica e Scienze della Terra, Università degli Studi di Ferrara, Via Saragat 1, I-44122 Ferrara, Italy
[17] Dipartimento di Fisica "E.R. Caianiello", Università degli Studi di Salerno, Via Giovanni Paolo II, I-84084 Fisciano (SA), Italy
Received 2022 July 27; revised 2022 December 10; accepted 2022 December 12; published 2023 January 10

Abstract

How passive galaxies form, and the physical mechanisms which prevent star formation over long timescales, are some of the most outstanding questions in understanding galaxy evolution. The properties of quiescent galaxies over cosmic time provide crucial information to identify the quenching mechanisms. Passive galaxies have been confirmed and studied out to $z \sim 4$, but all of these studies have been limited to massive systems (mostly with $\log(M_{\rm star}/M_{\odot}) > 10.8$). Using JWST-NIRISS grism slitless spectroscopic data from the GLASS-JWST Early Release Science program, we present spectroscopic confirmation of two quiescent galaxies at $z_{\rm spec} = 2.650^{+0.004}_{-0.006}$ and $z_{\rm spec} = 2.433^{+0.032}_{-0.016}$ (3σ errors) with stellar masses of $\log(M_{\rm star}/M_{\odot}) = 10.59^{+0.11}_{-0.05}$ and $\log(M_{\rm star}/M_{\odot}) = 10.07^{+0.06}_{-0.03}$ (corrected for magnification factors of $\mu = 2.0$ and $\mu = 2.1$, respectively). The latter represents the first spectroscopic confirmation of the existence of low-mass quiescent galaxies at cosmic noon, showcasing the power of JWST to identify and characterize this enigmatic population.

Unified Astronomy Thesaurus concepts: Galaxies (573); High-redshift galaxies (734); Quenched galaxies (2016)

1. Introduction

Two of the most outstanding questions in understanding galaxy evolution are how quiescent galaxies form and what mechanisms are responsible for the halting of the star formation activity. Several physical processes and theoretical explanations have been suggested to first stop star formation in a galaxy and then maintain it as quiescent over its lifetime (see Man & Belli 2018 for a brief review of quenching mechanisms). The properties of quiescent galaxies as a function of cosmic time (e.g., stellar mass function and number density, star formation history, stellar age, metallicity, [α/Fe] abundance, size and morphology, kinematics, and environment) provide crucial information to identify the quenching mechanisms and their relative importance at different times in the cosmic history.

Over the last decade, incredibly dedicated effort and investment on ground-based 8–10 m telescopes and the Hubble Space Telescope (HST) have repeatedly pushed the spectroscopic confirmation of the existence of quiescent galaxies to $z \sim 4$, when the universe was only 1.5 Gyr old, progressively challenging theoretical models of galaxy formation and evolution (Gobat et al. 2012; Marsan et al. 2015; Glazebrook et al. 2017; Kado-Fong et al. 2017; Forrest et al. 2020a). Multiobject deep near-IR (NIR) (i.e., rest-frame optical) spectroscopy of $2 < z < 4$ quiescent galaxies has allowed for the measurements of their stellar populations and star formation histories (Schreiber et al. 2018; Belli et al. 2019; D'Eugenio et al. 2020, 2021; Estrada-Carpenter et al. 2020; Forrest et al. 2020a, 2020b; Saracco et al. 2020; Valentino et al. 2020), kinematics, sizes, and morphologies (van de Sande et al. 2013; Belli et al. 2017; Hill et al. 2016; Newman et al. 2018; Tanaka et al. 2019; Estrada-Carpenter et al. 2020; Saracco et al. 2020; Esdaile et al. 2021; Stockmann et al. 2021; Forrest et al. 2022), metallicity (Morishita et al. 2019; Saracco et al. 2020), [α/Fe] abundances (Kriek et al. 2016), and environment (McConachie et al. 2022).

However, all of these studies have been limited to the most massive quiescent galaxies (mostly $\log(M_{\rm star}/M_\odot) > 11$, with only a small fraction with $10.5 < \log(M_{\rm star}/M_\odot) < 11$). No low-mass (i.e., $\log(M_{\rm star}/M_\odot) < 10.5$, hereafter corresponding to around a third of the characteristic stellar mass of the galaxy stellar mass function; e.g., Muzzin et al. 2013) quiescent galaxy at $z > 2$ has been spectroscopically confirmed yet, preventing the exploration of quenching mechanisms to the low-stellar-mass regime at cosmic noon. For example, while some form of feedback generally attributed to active galactic nuclei (AGNs) is supposed for the quenching of galaxies at the massive end, it is unclear whether AGN feedback can also operate in low-mass galaxies. Furthermore, halo quenching is not expected to operate in dark matter halos below $10^{12}\,M_\odot$ at $z \approx 2$ (Dekel & Birnboim 2008), corresponding to roughly $M_{\rm star} \sim 10^{10.5}\,M_\odot$ (Behroozi et al. 2013). Indeed, multiwavelength photometric surveys have been able to push photometric measurements of the stellar mass function of quiescent galaxies down to $\log(M_{\rm star}/M_\odot) \sim 9.5$–$10$ at $z \approx 2$–3, finding a sharp decline in the number density of quiescent galaxies with $\log(M_{\rm star}/M_\odot) \lesssim 10.5$ (e.g., Tomczak et al. 2014), although spectroscopic redshift measurements are needed to confirm these findings.

The advent of the JWST, with its amazing set of instruments, finally enables us to definitively identify low-mass quiescent galaxies at $z > 2$ and to spectroscopically characterize their properties for the first time.

In this Letter, we present spectroscopic confirmation of two quiescent galaxies at $z > 2$, including the first spectroscopic confirmation of a low-mass quiescent galaxy at $z > 2$, using JWST-NIRISS grism slitless spectroscopic data obtained from the GLASS-JWST Early Release Science (ERS-1324; PI: Treu) program. GLASS-JWST is obtaining NIRISS (Doyon et al. 2012; Willott et al. 2022) and NIRSpec (Jakobsen et al. 2022) spectroscopy in the center of the A2744 cluster field, while obtaining NIRCAM (Rieke et al. 2005) images of two parallel fields. GLASS-JWST consists of the deepest extragalactic data among the ERS programs. Details can be found in the survey paper (Treu et al. 2022).

This Letter is organized as follows. In Section 2 we introduce the selection of the low-mass quiescent galaxy candidates from multiwavelength photometric catalogs in the A2744 cluster field. In Section 3 we present the JWST-NIRISS grism spectra of the low-mass quiescent galaxies, their spectroscopic redshifts, robust stellar masses obtained from the modeling of the photometry, and gravitational lensing magnification corrections. We conclude in Section 4. Magnitudes are given in the AB system and a standard cosmology with $\Omega_{\rm m} = 0.3$, $\Omega_\Lambda = 0.7$, and $h = 0.7$ is assumed when necessary, along with a Chabrier (2003) initial mass function.

2. Sample of Low-mass Quiescent Galaxies

Candidate low-mass quiescent galaxies were selected from the HFF-DeepSpace catalogs in the Abell 2744 cluster (hereafter, A2744-clu) pointing constructed by Shipley et al. (2018), and cross-validated using the HFF-ASTRODEEP catalogs (Castellano et al. 2016; Merlin et al. 2016).

The NIR-selected HFF-DeepSpace A2744-clu photometric catalog covers an area of $\sim$5.4 arcmin^2 with complete coverage in 14 bands from the HST-UVIS F275W to the Spitzer-IRAC 8 μm down to a 75% detection completeness of $\sim$28.2 mag in the F160W band. EAZY (Brammer et al. 2008) was used to derive photometric redshifts ($z_{\rm phot}$) and rest-frame colors. Fitting and Assessment of Synthetic Templates (FAST; Kriek et al. 2009) was used to derive stellar population properties adopting Bruzual & Charlot (2003) stellar population synthesis models, a delayed exponentially declining star formation history (SFH),[18] solar metallicity, and a Calzetti et al. (2000) dust attenuation law with $0 < A_V[{\rm mag}] < 6$. See Shipley et al. (2018) for a detailed description of the HFF-DeepSpace catalogs and high-level science data.

First, we selected all galaxies with $m_{\rm F160W} < 26.5$, photometric redshift $z_{\rm phot} > 2$, stellar mass $M_{\rm star} > 10^8\ M_\odot$, and specific star formation rate (sSFR) $\log({\rm sSFR}[{\rm yr}^{-1}]) < -9.7$, and use_phot = 1.[19] We then visually inspected postage stamps of the HST images, detection image, and segmentation map of all resulting objects using the HFFexplorer[20] to remove any spurious or problematic objects (e.g., galaxies contaminated by stellar diffraction spikes, objects detected too close to subtracted bright cluster galaxies, very broad/unconstrained photometric redshift probability functions, blended objects, and potentially merging systems). This resulted in 25 galaxies, shown in the sSFR–$M_{\rm star}$ diagram (Figure 1, top panel) and in the rest-frame $U-V$ versus $V-J$ diagram (Figure 1, bottom panel; hereafter, *UVJ* diagram).

Candidate quiescent galaxies were finally selected based on their positions within (or close to the boundary of) the quiescent wedge in the *UVJ* diagram and from visual inspection of their spectral energy distributions (SEDs), looking for strong rest-frame optical Balmer/4000 Å breaks. A few additional objects with poorly sampled SEDs around the rest-frame optical breaks were removed from the initial sample. This resulted in the identification of eight low-mass quiescent galaxies, shown as filled colored circles in Figure 1. Their SEDs are shown in Figure 2, while Table 1 lists their photometrically derived properties.

Several works (e.g., Marsan et al. 2015; Merlin et al. 2018, 2019; Schreiber et al. 2018; Carnall et al. 2020) have shown that the standard selection of quiescent galaxies in the *UVJ* diagram (in particular, the $U-V > 1.3$ criterion) is potentially biased against unobscured recently quenched (i.e., younger than a few hundred million years) post-starburst galaxies, which still have significant emission in the UV due to massive bright stars not yet being evolved off the main sequence (see, e.g., ID = 5715 in Figure 2). Here we apply a conservative approach, selecting unambiguous evolved quiescent galaxies, and we postpone a systematic and complete search for quiescent distant galaxies to future studies.

3. Analysis and Results

The GLASS-ERS program, executed on 2022 June 28–29, performed wide-field slitless spectroscopy at 1.0–2.2 μm with NIRISS with a single pointing roughly centered on the core of A2744-clu. The reduction of the NIRISS data, along with the extraction of the spectra and modeling of the contamination, performed with the `Grizli`[21] analysis software (Brammer & Matharu 2021), is presented in another companion paper (Roberts-Borsani et al. 2022, hereafter Paper I).

[18] SFR $\propto t\, e^{-t/\tau}$.

[19] The flag use_phot = 1 excludes stars, sources close to a bright star, sources with signal-to-noise ratio < 3 in the F160W band, catastrophic photometric redshift fits, and catastrophic stellar population fits; see Shipley et al. (2018).

[20] http://cosmos.phy.tufts.edu/~danilo/HFF/HFFexplorer/

[21] https://github.com/gbrammer/grizli

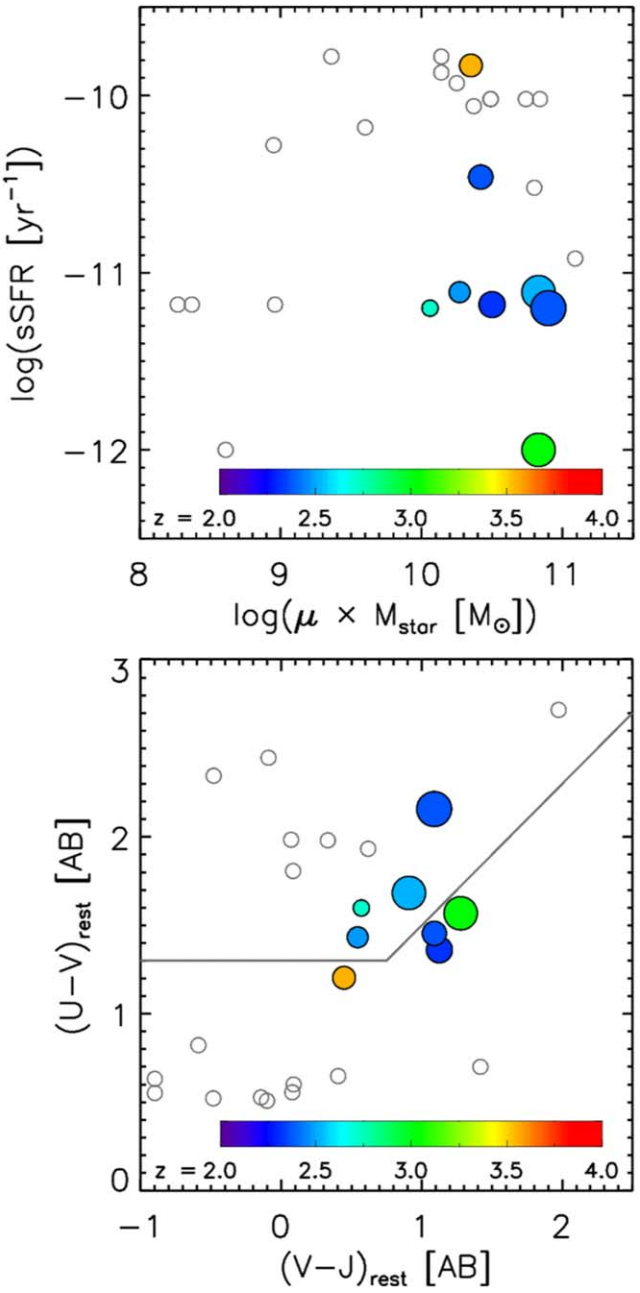

Figure 1. Top: the sSFR vs. $M_{\rm star}$ diagram of galaxies selected as explained in Section 2. The candidates of low-mass quiescent galaxies at $z > 2$ are shown color-coded as a function of redshift; larger colored filled circles indicate larger stellar masses. Bottom: *UVJ* diagram of the same galaxies plotted in the top panel, with the quiescent wedge as defined in Martis et al. (2016) plotted in gray. Eight robust candidates of low-mass quiescent galaxies at $z > 2$ are identified.

Of the eight candidates listed in Table 1, three (IDs = 1412, 2500, and 4111) are outside of the NIRISS pointing, whereas three others (IDs = 6555, 1103, and 5715) have a significant level of contamination from bright nearby sources which cannot be optimally corrected for with the current preliminary calibration files (see Paper I for details). The `Grizli` extracted one-dimensional NIRISS spectra of the remaining two candidates are shown in Figure 3, along with their false-color images constructed from both HST-WFC3/NIR bands and JWST-NIRISS bands separately. Although ID = 4877 is the most massive quiescent candidate of the sample, with $\log(M_{\rm star}^{\rm corr}/M_\odot) = 10.67$, it is comparable to the lowest mass quiescent galaxy spectroscopically confirmed at $z > 2$ to date (Estrada-Carpenter et al. 2020). On the other hand, ID = 5607, with $\log(M_{\rm star}^{\rm corr}/M_\odot) = 9.92$, pushes the limit well below previous works, since it has a stellar mass estimate before lensing magnification correction $<10^{10.5}\ M_\odot$.

Figure 3 shows the best-fit `Grizli` model (red curve) which places them, respectively, at redshifts of $z_{\rm spec} = 2.650^{+0.004}_{-0.006}$ and $z_{\rm spec} = 2.433^{+0.032}_{-0.016}$ (3σ errors). The NIRISS spectra show strong Balmer/4000 Å breaks, as well as other blended stellar continuum absorption features (the locations of Ca II HK, Hδ, Hγ, Hβ, Mgb, and NaD are highlighted in Figure 3). Furthermore, the NIRISS spectra do not show evidence of emission lines, confirming the quiescent nature of the candidates. For ID = 4877, emission-line forced photometry returns $f_{\rm [O\,II]} = 0.2(\pm 1.5) \times 10^{-18}$ erg s^{-1} cm^{-2}, $f_{\rm H\beta} = 1.4(\pm 2.1) \times 10^{-18}$ erg s^{-1} cm^{-2}, and $f_{\rm [O\,III]} = 4.6(\pm 2.5) \times 10^{-18}$ erg s^{-1} cm^{-2}, whereas for ID = 5607 we measure $f_{\rm [O\,II]} = -4.7(\pm 1.2) \times 10^{-18}$ erg s^{-1} cm^{-2}, $f_{\rm H\beta} = -0.2(\pm 2.3) \times 10^{-18}$ erg s^{-1} cm^{-2}, although both [O II] and Hβ are right at the longer-wavelength end of the F115W and F150W spectra, respectively, whereas [O III] falls in the gap between F150W and F200W.

We used FAST to model the HFF-DeepSpace photometry combined with the NIRISS F115W, F150W, and F200W spectra, fixing the redshift at the spectroscopic redshift. Compared to the SED-modeling assumptions presented in Section 2, we allowed for a range of stellar metallicities from subsolar ($Z = 0.004$) to supersolar ($Z = 0.05$). Figure 3 shows in blue the best-fit FAST model.

The best-fit stellar masses (not corrected for lensing magnification factor μ) at the spectroscopic redshifts are $\log(\mu \times M_{\rm star}/M_\odot) = 10.89^{+0.10(0.11)}_{-0.04(0.05)}$ and $10.38^{+0.05(0.08)}_{-0.02(0.03)}$ (1(3) σ uncertainties) for ID = 4877 and ID = 5607, respectively, in good agreement within the errors with those previously determined adopting the photometric redshifts. The SED modeling confirms the quiescent nature of these two candidates, with 3σ upper limits on the star formation rates of SFR < 0.1–$0.2\ M_\odot$ yr^{-1}, and on the sSFR of $\log({\rm sSFR[yr^{-1}]}) < -12$ and <-11.1, for ID = 4877 and ID = 5607, respectively, compared to $\log({\rm sSFR[yr^{-1}]}) > -8.8$ for typical main-sequence star-forming galaxies at $2.0 < z < 2.5$ with similar stellar masses (Whitaker et al. 2014).

Using revised lensing magnification maps from Bergamini et al. (2022) and adopting the spectroscopic redshifts, we find $\mu_{\rm spec} = 2.02 \pm 0.04$ and $\mu_{\rm spec} = 2.09 \pm 0.05$ for ID = 4877 and ID = 5607, respectively. We note that this does not include systematic uncertainty arising from lens-modeling assumptions, although we expect this uncertainty to be modest given the magnification factors. The gravitational lensing magnification corrected stellar masses are therefore found to be $\log(M_{\rm star}^{\rm corr}/M_\odot) = 10.59^{+0.11}_{-0.05}$ for ID = 4877 and $\log(M_{\rm star}^{\rm corr}/M_\odot) = 10.07^{+0.06}_{-0.03}$ for ID = 5607 (1σ uncertainties). With a stellar mass of $\approx 10^{10}\ M_\odot$, HFF-DS 5607 is the lowest mass quiescent galaxy to be spectroscopically confirmed at $z > 2$ to date.

The addition of the NIRISS spectra to the photometry in the SED modeling results in significantly better constrained stellar population properties, as shown in Figure 4. In particular, moderate dust extinction $A_V \sim 0.5$ mag is found to be present in both galaxies. The stellar age is robustly constrained for both sources to be in the range $\sim$0.8–1.3 Gyr (3σ) while the timescale τ of the SFH is found to be quite short, with a 3σ

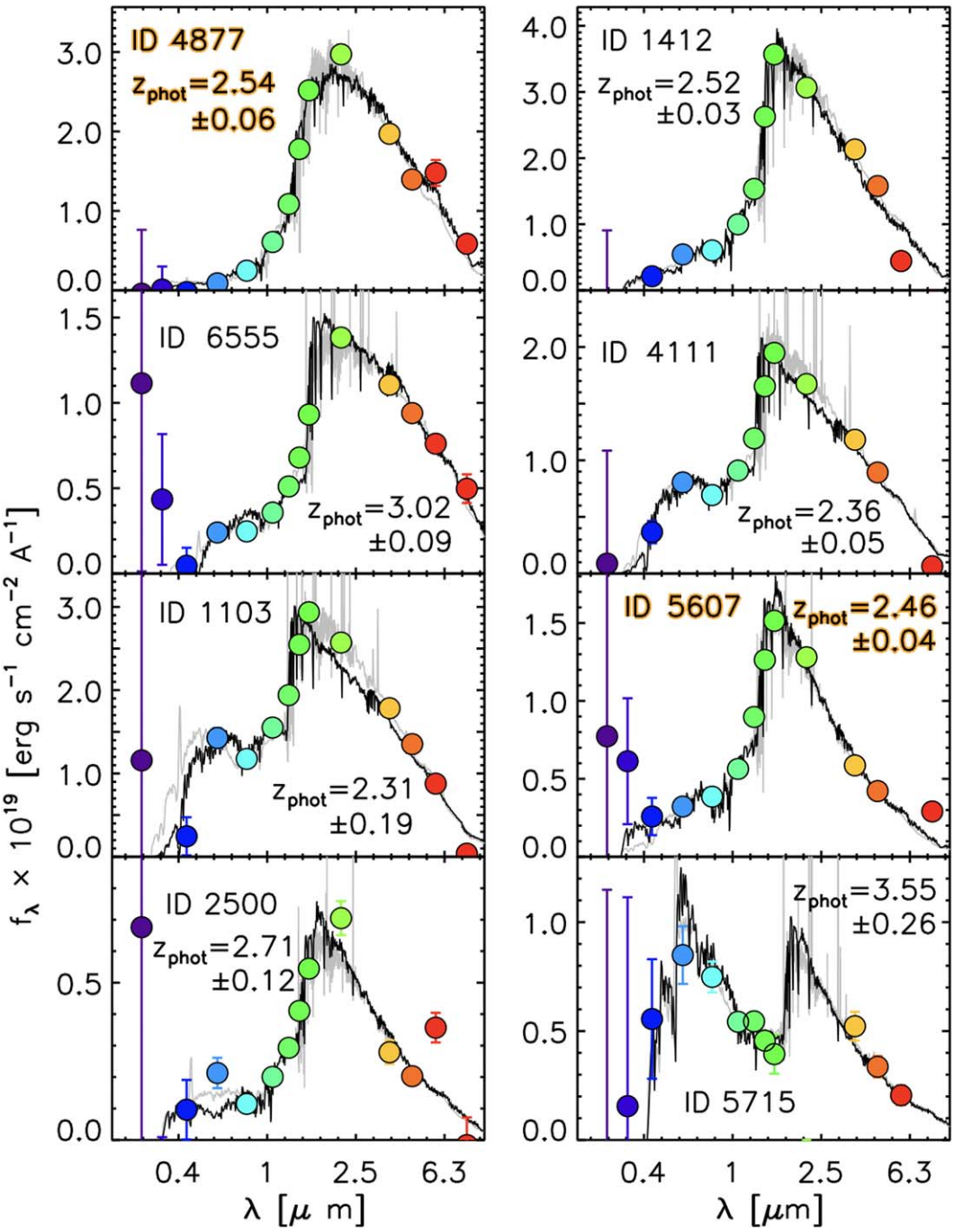

Figure 2. SEDs of the selected candidates of low-mass quiescent galaxies at $z > 2$. Filled colored circles represent the observed HFF-DeepSpace photometry; the gray and black curves show the best-fit EAZY and FAST models, respectively. The photometric redshifts and the corresponding 1σ errors are listed. The two galaxies (IDs = 4877 and 5607) with NIRISS spectroscopy presented in this Letter are highlighted in orange.

upper limit of 100 Myr for both sources, indicative of a rapid formation for both low-mass quiescent galaxies. We note that the detailed fits and derived stellar population properties are model dependent, and we expect these to improve with more sophisticated modeling (e.g., adopting nonparametric SFHs) and improved calibration of the NIRISS data.

4. Summary and Conclusions

This Letter presents a first look at low-mass quiescent galaxies in the JWST-NIRISS data from the GLASS-ERS survey in the A2744 cluster. The power of JWST for spectroscopic studies of low-mass quiescent galaxies at cosmic noon (i.e., $z > 2$) is demonstrated by spectroscopic confirmation of the quiescent nature of two $z \sim 2.5$ galaxies, which were identified through SED modeling as passive candidates in the HFF-DeepSpace photometric catalogs. Our results are summarized as follows:

1. We measure the spectroscopic redshifts of two low-mass quiescent galaxies via their Balmer/4000 Å breaks and stellar absorption features from NIRISS spectra ($z = 2.650^{+0.004}_{-0.006}$ for HFF-DS 4877 and $z = 2.433^{+0.032}_{-0.016}$ for HFF-DS 5607; 3σ errors).

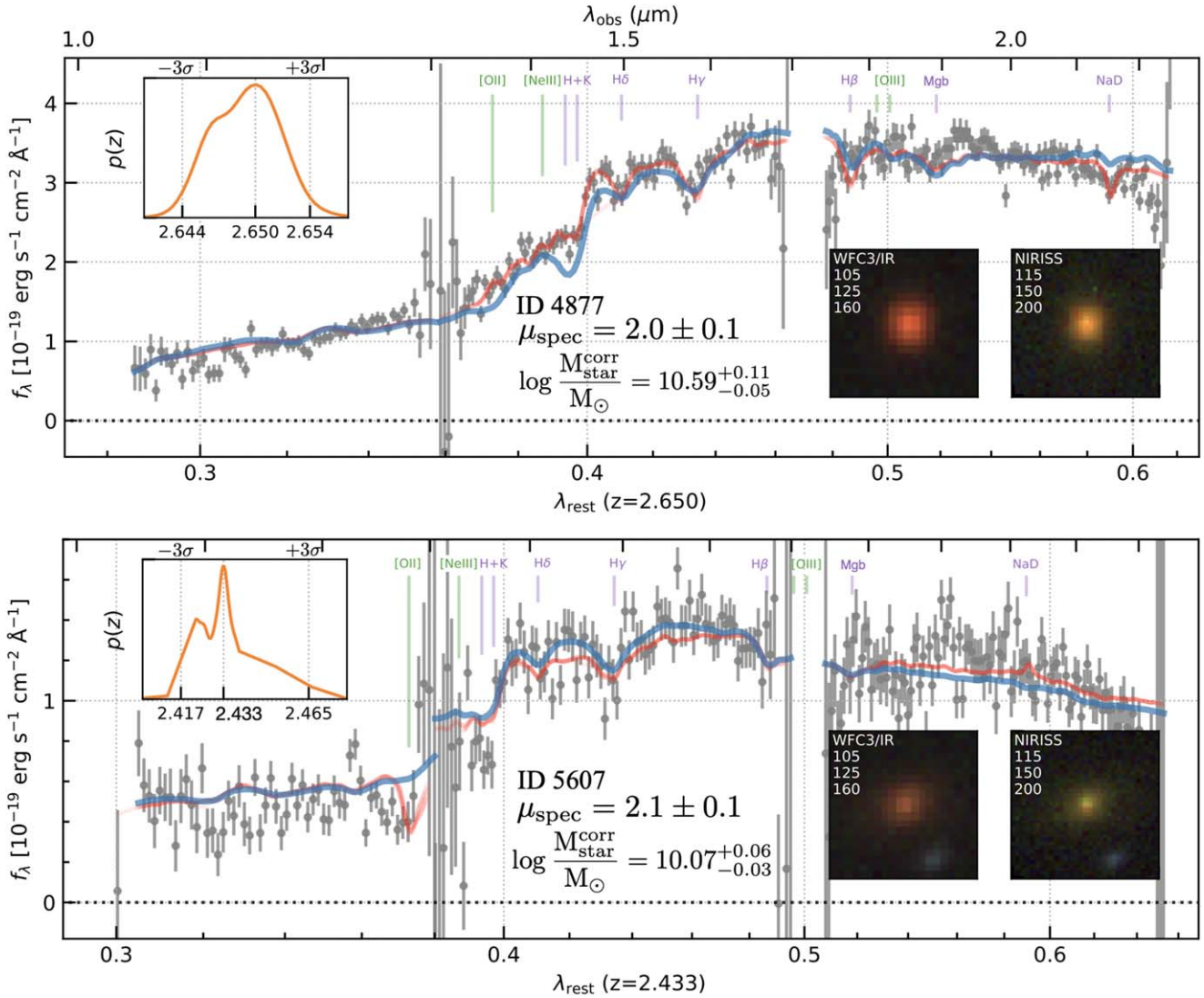

Figure 3. Top: NIRISS F115W+F150W+F200W spectrum of HFF-DS 4877 (gray symbols) with `Grizli` best-fit model (red solid curve) and FAST best-fit model (blue solid curve) overplotted. The positions of major spectral features (e.g., [O II], Ca II HK, Hδ, Hγ, Hβ, [O III], Mgb, and NaD) are highlighted at the best-fit `Grizli` redshift. The gravitational lensing magnification factor and stellar mass, corrected for lensing magnification, derived assuming the spectroscopic redshift are listed. The top-left inset shows the `Grizli` redshift probability function $p(z)$ in orange, with listed the best-fist `Grizli` spectroscopic redshift and upper and lower 3σ values. The bottom-right insets show false-color images ($2'' \times 2''$) from HST-WFC3/NIR bands (left) and JWST-NIRISS bands (right). Bottom: same as the top panel, but for HFF-DS 5607. With a gravitational lensing corrected stellar mass below $10^{10}\,M_{\odot}$, HFF-DS 5607 is the first low-mass quiescent galaxy spectroscopically confirmed at $z > 2$.

Table 1
Sample of Selected Candidates of Low-mass Quiescent Galaxies at $z > 2$ and their Properties (from Shipley et al. 2018)

ID (HFF-DS)	R.A. (deg)	Decl. (deg)	H_{160} (AB)	$z_{\rm phot}$	$\log(\mu \times M_{\rm star})$ ($M_{\odot}$)	log(sSFR) ($\rm yr^{-1}$)	μ	$\log(M_{\rm star}^{\rm corr})$ ($M_{\odot}$)
4877[a]	3.605219	−30.39540	23.15	2.54 ± 0.06	10.97	−11.20	$2.0^{+0.1}_{-0.1}$	10.67
1412	3.575537	−30.41321	22.77	2.52 ± 0.03	10.83	−11.11	$2.1^{+0.1}_{-0.1}$	10.52
6555	3.582519	−30.38545	24.23	3.02 ± 0.09	10.83	−12.00	$4.0^{+0.1}_{-0.1}$	10.23
4111	3.568355	−30.39953	23.43	2.36 ± 0.05	10.42	−10.46	$2.3^{+0.1}_{-0.1}$	10.06
1103	3.585363	−30.41533	22.98	2.31 ± 0.19	10.50	−11.18	$2.8^{+0.1}_{-0.1}$	10.06
5607[a]	3.601594	−30.39150	23.70	2.46 ± 0.04	10.24	−11.11	$2.1^{+0.1}_{-0.1}$	9.92
2500	3.572230	−30.40686	24.81	2.71 ± 0.12	10.06	−11.20	$2.2^{+0.1}_{-0.1}$	9.73
5715	3.586502	−30.39048	25.16	3.55 ± 0.26	10.35	−9.83	$9.1^{+1.1}_{-0.6}$	9.39

Notes. Derived adopting the listed photometric redshifts $z_{\rm phot}$ (with 1σ uncertainties). $\log(M_{\rm star}^{\rm corr})$ lists the stellar mass after correcting for the listed gravitational lensing magnification factors μ from Bergamini et al. (2022); the quoted uncertainties on μ are 1σ statistical errors.
[a] The two galaxies with NIRISS spectroscopy presented in this Letter.

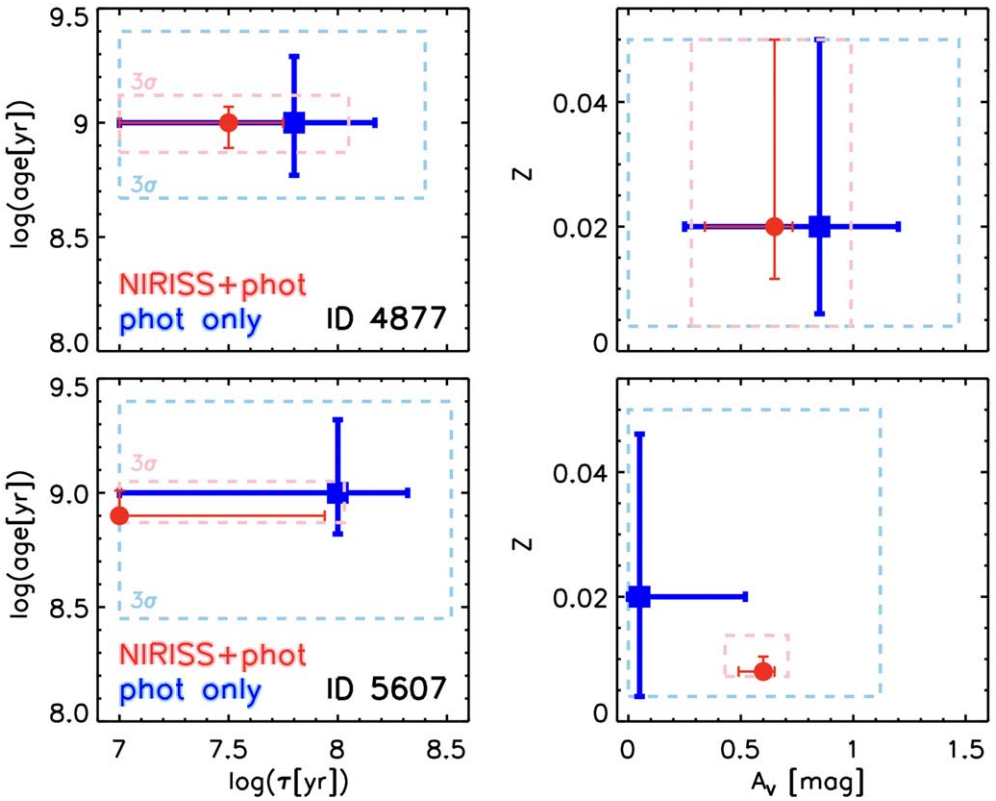

Figure 4. Stellar population properties (stellar age vs. τ, left panels; stellar metallicity vs. dust obscuration, right panels) and corresponding errors derived from modeling the photometry alone (blue square and error bars, cyan dashed box) and the photometry combined with the NIRISS spectroscopy (red circle and error bars, pink dashed box). Error bars represent 1σ uncertainties, while the dashed boxes represent 1σ errors. Top panels show the results for ID = 4877; bottom panels show the results from ID = 5607.

2. The quiescent nature of the two galaxies is further confirmed by SED modeling of the combined photometry and NIRISS spectra, resulting in SFR $< 0.2\,M_{\odot}$ yr^{-1} and $\log(\mathrm{sSFR}[\mathrm{yr}^{-1}]) < -11$, i.e., star formation activity suppressed by more than two orders of magnitude compared to typical star-forming galaxies with similar masses at $2.0 < z < 2.5$.
3. No nebular emission lines (i.e., [O II], Hβ, and [O III]) are detected in the spectra, further supporting the quiescent nature of these two galaxies.
4. HFF-DS 5607, with a gravitational lensing magnification corrected stellar mass $\log(M_{\mathrm{star}}^{\mathrm{corr}}/M_{\odot}) = 10.07^{+0.06}_{-0.03}$, is the first spectroscopically confirmed low-mass quiescent galaxy at $z > 2$.
5. The combination of NIRISS spectroscopy and photometry of distant, low-mass quiescent galaxies is shown to enable the robust measurements of their stellar population properties, such as stellar age, SFH, and dust obscuration.

JWST is finally allowing us, for the first time, to spectroscopically identify and study the population of low-mass ($\log(M_{\mathrm{star}}/M_{\odot}) < 10.5$) quiescent galaxies at $z > 2$. The extension of these studies to large and complete sample of low-mass quiescent galaxies will allow for the first spectroscopic measurement of the number density of distant, low-mass quiescent galaxies, and will provide crucial information to discriminate between the multiple quenching mechanisms characterized by different timescales, investigating their potential dependency on stellar mass.

This work is based on observations made with the NASA/ESA/CSA JWST. The data were obtained from the Mikulski Archive for Space Telescopes at the Space Telescope Science Institute, which is operated by the Association of Universities for Research in Astronomy, Inc., under NASA contract NAS 5-03127 for JWST. These observations are associated with program JWST-ERS-1324. Support for program GLASS-JWST ERS-1324 was provided by NASA through a grant from the Space Telescope Science Institute, which is operated by the Association of Universities for Research in Astronomy, Inc., under NASA contract NAS 5-03127. D.M. and C.T. acknowledge financial support from program HST-GO-17231, provided through a grant from the STScI under NASA contract NAS5-26555. PS acknowledges INAF Mini Grant 2022 "The evolution of passive galaxies through cosmic time". K.G. and T.N. acknowledge support from Australian Research Council Laureate Fellowship FL180100060. We acknowledge financial support through grants PRIN-MIUR 2017WSCC32 and 2020SKSTHZ. AA has received funding from the European Union's Horizon 2020 Research and Innovation Programme under the Marie Skłodowska-Curie grant agreement No 101024195 — ROSEAU. M.B. acknowledges support from the Slovenian national research agency ARRS through grant N1-0238. This work is based on data and catalog products from HFF-DeepSpace, funded by the National Science Foundation and Space Telescope Science Institute (operated by the Association of Universities for Research in Astronomy Inc., under NASA contract NAS5-26555). The Cosmic Dawn Center is funded by the Danish National Research Foundation

(DNRF) under grant No. 140. Cloud-based data processing and file storage for this work is provided by the AWS Cloud Credits for Research program.

ORCID iDs

Danilo Marchesini https://orcid.org/0000-0001-9002-3502
Gabriel Brammer https://orcid.org/0000-0003-2680-005X
Takahiro Morishita https://orcid.org/0000-0002-8512-1404
Pietro Bergamini https://orcid.org/0000-0003-1383-9414
Xin Wang https://orcid.org/0000-0002-9373-3865
Marusa Bradac https://orcid.org/0000-0001-5984-0395
Guido Roberts-Borsani https://orcid.org/0000-0002-4140-1367
Victoria Strait https://orcid.org/0000-0002-6338-7295
Tommaso Treu https://orcid.org/0000-0002-8460-0390
Adriano Fontana https://orcid.org/0000-0003-3820-2823
Tucker Jones https://orcid.org/0000-0001-5860-3419
Paola Santini https://orcid.org/0000-0002-9334-8705
Benedetta Vulcani https://orcid.org/0000-0003-0980-1499
Ana Acebron https://orcid.org/0000-0003-3108-9039
Antonello Calabrò https://orcid.org/0000-0003-2536-1614
Marco Castellano https://orcid.org/0000-0001-9875-8263
Karl Glazebrook https://orcid.org/0000-0002-3254-9044
Claudio Grillo https://orcid.org/0000-0002-5926-7143
Amata Mercurio https://orcid.org/0000-0001-9261-7849
Themiya Nanayakkara https://orcid.org/0000-0003-2804-0648
Piero Rosati https://orcid.org/0000-0002-6813-0632
Chanita Tubthong https://orcid.org/0000-0002-7907-2634
Eros Vanzella https://orcid.org/0000-0002-5057-135X

References

Behroozi, P. S., Wechsler, R. H., & Conroy, C. 2013, ApJL, 762, L31
Belli, S., Newman, A. B., & Ellis, R. S. 2017, ApJ, 834, 18
Belli, S., Newman, A. B., & Ellis, R. S. 2019, ApJ, 874, 17
Bergamini, P., Acebron, A., Grillo, C., et al. 2022, arXiv:2207.09416
Brammer, G., & Matharu, J. 2021, gbrammer/grizli: Release 2021, v1.3.2, Zenodo, doi:10.5281/zenodo.1146904
Brammer, G. B., van Dokkum, P. G., & Coppi, P. 2008, ApJ, 686, 1503
Bruzual, G., & Charlot, S. 2003, MNRAS, 344, 1000
Calzetti, D., Armus, L., Bohlin, R. C., et al. 2000, ApJ, 533, 682
Carnall, A. C., Walker, S., McLure, R. J., et al. 2020, MNRAS, 496, 695
Castellano, M., Amorín, R., Merlin, E., et al. 2016, A&A, 590, A31
Chabrier, G. 2003, PASP, 115, 763
Dekel, A., & Birnboim, Y. 2008, MNRAS, 383, 119
D'Eugenio, C., Daddi, E., Gobat, R., et al. 2020, ApJL, 892, L2
D'Eugenio, C., Daddi, E., Gobat, R., et al. 2021, A&A, 653, A32
Doyon, R., Hutchings, J. B., Beaulieu, M., et al. 2012, Proc. SPIE, 8442, 84422R
Esdaile, J., Glazebrook, K., Labbé, I., et al. 2021, ApJL, 908, L35
Estrada-Carpenter, V., Papovich, C., Momcheva, I., et al. 2020, ApJ, 898, 171
Forrest, B., Annunziatella, M., Wilson, G., et al. 2020a, ApJL, 890, L1
Forrest, B., Marsan, Z. C., Annunziatella, M., et al. 2020b, ApJ, 903, 47
Forrest, B., Wilson, G., Muzzin, A., et al. 2022, ApJ, 938, 109
Glazebrook, K., Schreiber, C., Labbé, I., et al. 2017, Natur, 544, 71
Gobat, R., Strazzullo, V., Daddi, E., et al. 2012, ApJL, 759, L44
Hill, A., Muzzin, A., Franx, M., & van de Sande, J. 2016, ApJ, 819, 74
Jakobsen, P., Ferruit, P., Alves de Oliveira, C., et al. 2022, A&A, 661, A80
Kado-Fong, E., Marchesini, D., Marsan, Z. C., et al. 2017, ApJ, 838, 57
Kriek, M., Conroy, C., van Dokkum, P. G., et al. 2016, Natur, 540, 248
Kriek, M., van Dokkum, P. G., Labbé, I., et al. 2009, ApJ, 700, 221
Man, A., & Belli, S. 2018, NatAs, 2, 695
Marsan, Z. C., Marchesini, D., Brammer, G. B., et al. 2015, ApJ, 801, 133
Martis, N. S., Marchesini, D., Brammer, G. B., et al. 2016, ApJL, 827, L25
McConachie, I., Wilson, G., Forrest, B., et al. 2022, ApJ, 926, 37
Merlin, E., Amorín, R., Castellano, M., et al. 2016, A&A, 590, A30
Merlin, E., Fontana, A., Castellano, M., et al. 2018, MNRAS, 473, 2098
Merlin, E., Fortuni, F., Torelli, M., et al. 2019, MNRAS, 490, 3309
Morishita, T., Abramson, L. E., Treu, T., et al. 2019, ApJ, 877, 141
Muzzin, A., Marchesini, D., Stefanon, M., et al. 2013, ApJ, 777, 18
Newman, A. B., Belli, S., Ellis, R. S., & Patel, S. G. 2018, ApJ, 862, 125
Rieke, M. J., Heaney, J. B., Burriesci, L. G., Kelly, D., & Horner, S. 2005, Proc. SPIE, 5904, 1
Roberts-Borsani, G., Morishita, T., Treu, T., et al. 2022, ApJL, 938, L13
Saracco, P., Marchesini, D., Barbera, F. L., et al. 2020, ApJ, 905, 40
Schreiber, C., Glazebrook, K., Nanayakkara, T., et al. 2018, A&A, 618, A85
Shipley, H. V., Lange-Vagle, D., Marchesini, D., et al. 2018, ApJS, 235, 14
Stockmann, M., Jørgensen, I., Toft, S., et al. 2021, ApJ, 908, 135
Tanaka, M., Valentino, F., Toft, S., et al. 2019, ApJL, 885, L34
Tomczak, A. R., Quadri, R. F., Tran, K.-V.-H., et al. 2014, ApJ, 783, 85
Treu, T., Roberts-Borsani, G., Bradac, M., et al. 2022, ApJ, 935, 110
Valentino, F., Tanaka, M., Davidzon, I., et al. 2020, ApJ, 889, 93
van de Sande, J., Kriek, M., Franx, M., et al. 2013, ApJ, 771, 85
Whitaker, K. E., Franx, M., Leja, J., et al. 2014, ApJ, 795, 104
Willott, C. J., Doyon, R., Albert, L., et al. 2022, PASP, 134, 025002